Journal of Hazardous Materials 184 (2010) 147–155

Contents lists available at ScienceDirect

Journal of Hazardous Materials

journal homepage: www.elsevier.com/locate/jhazmat

Benzotriazole removal from water by Zn–Al–O binary metal oxide adsorbent: Behavior, kinetics and mechanism

Bingbing Xu, Fengchang Wu*, Xiaoli Zhao, Haiqing Liao

State Environmental Protection Key Laboratory for Lake Pollution Control, Chinese Research Academy of Environmental Sciences, Beijing 100012, China

ARTICLE INFO

Article history:
Received 17 January 2010
Received in revised form 29 July 2010
Accepted 6 August 2010
Available online 14 August 2010

Keywords:
Benzotriazole
Polar contaminant
Zn–Al–O binary metal oxide
Adsorption

ABSTRACT

In this study, a novel Zn–Al–O binary metal oxide adsorbent was prepared and used to remove the emerging polar contaminant benzotriazole from water. The adsorption behavior, kinetics and mechanism were systemically studied. Results showed that benzotriazole was rapidly and effectively adsorbed by the adsorbent. Instantaneous adsorption was observed under each studied condition, and the adsorption reached equilibrium within 30 min. High initial benzotriazole concentration enhanced the adsorption. The amount of absorbed benzotriazole increased with increasing adsorbent dosage, but decreased with increasing ionic strength. Solution pH had little effect on benzotriazole adsorption. The adsorption isotherm was consistent with S-type. Langmuir isotherm model fitted the equilibrium data better than Freundlich, Dubinin–Radushkevich and Temkin isotherm models. The maximum monolayer adsorptive capacity of benzotriazole with and without electrolytes was 7.30 mg g^{-1} and 9.51 mg g^{-1}, respectively. Elovich and pseudo-second-order models were most suitable for describing the adsorption kinetics. Interactions between the surface sites of the adsorbent and benzotriazole may be a combination of electrostatic interaction, ion exchange and hydrogen bond.

1. Introduction

With a large number of applications of synthetic chemicals in human daily lives, as well as in industrial and agricultural production, various emerging contaminants are continually being identified. Benzotriazole is a typical emerging contaminant [1]. Benzotriazole and its methyl substituted compounds are regarded as potential hazards to aquatic organisms, and can cause long-term adverse effects in aquatic environments [2,3].

Benzotriazole first became a concern because of the contamination caused by aircraft deicing fluids of which the primary agents were benzotriazole and its derivatives [4]. However, aircraft deicing fluids are only one of the common uses of benzotriazole. As a class of important industrial auxiliary chemicals, benzotriazole is widely used as a corrosion inhibitor, anti-freeze, UV absorber and anti-fog agents [2,3,5,6]. The annual production of benzotriazole is approximately 9000 tons worldwide [7]. Due to its extensive uses, benzotriazole becomes a class of widespread environmental contaminants. It has been detected in seven rivers in Switzerland, with a maximum concentration of 6.3 μg L^{-1}, giving a maximum contaminant flow of as much as 277 kg per week [3]. Benzotriazole was also detected in wastewater treatment plants in Germany with influent concentrations of 12 μg L^{-1} and effluent concentrations in the range of 7–18 μg L^{-1} [8,9].

Benzotriazole is characterized by a high water solubility (28 g L^{-1}), low vapor pressure, and low octanol water distribution coefficients ($\log K_{ow}$ = 1.23) [7]. It resists biodegradation and is only partially removed by wastewater treatment [9,10]. The removal efficiency of benzotriazole by conventional activated sludge was only 37% [7]. The treatment of municipal wastewater in a lab-scale membrane bioreactor slightly improved the benzotriazole removal efficiency. Ozonation is an effective method for degrading benzotriazole in water. Almost complete removal achieved by ozonation of the treatment plant effluent with 1 mg O_3• (mg DOC)$^{-1}$ [7]. However, there are some drawbacks associated with ozonation such as the complexity of the oxidation process, high costs, and uncertainty about the types and toxicity of by-products.

Adsorption technology becomes a mainstream method for water pollution control because of its low cost and easy operation. Metal oxides have been widely used as adsorbents due to their unique surface characteristics. Recent studies have reported the removal of various contaminants using metal oxides adsorbents, including arsenic [11–13], chromium [14], cadmium [15,16], dyes [17,18], fluoride [19–21] and many others.

The objectives of this work were to synthesize a novel adsorbent Zn–Al–O binary metal oxide and use it for benzotriazole removal from water to develop an available method for benzotriazole pollution control. Adsorption experiments were carried out as a function

* Corresponding author. Tel.: +86 10 84915312; fax: +86 10 84915277.
E-mail address: wufengchang@vip.skleg.cn (F. Wu).

0304-3894/$ – see front matter © 2010 Elsevier B.V. All rights reserved.
doi:10.1016/j.jhazmat.2010.08.017

of contact time, adsorbent dosage, solution pH, ionic strength and initial benzotriazole concentrations. Additionally, the removal efficiency, adsorption capacity, behavior, kinetics and mechanisms of benzotriazole adsorption on Zn–Al–O binary metal oxide were systematically evaluated.

2. Materials and methods

2.1. Reagents

Benzotriazole was purchased from Sigma–Aldrich, USA with purity greater than 98%. Other chemicals used in this study were of analytical reagent grade and were used without further purification. All stock solutions were prepared in deionized water.

All glassware used in the experiments was immersed in a solution of H_2SO_4–$K_2Cr_2O_7$ overnight, and was then washed several times in both tap water and distilled water.

2.2. Adsorbent preparation

The Zn–Al–O binary metal oxide that was used as the absorbent in this study was prepared using a co-precipitation method with a Zn:Al molar ratio of 2:1. Zinc nitrate hexahydrate (0.1 mol) and aluminum nitrate nonahydrate (0.05 mol) were dissolved in 200 mL deionized water, respectively. The two solutions were then mixed evenly in a water bath at a constant temperature of 80 °C. With vigorous magnetic-stirring, 20% NaOH solution was added drop wise into the mixture, and solution pH was strictly maintained in the range of 9.5–10. After addition of NaOH, the suspension was continuously stirred for 1 h and aged at room temperature for 24 h. Then the suspension was filtered and washed with deionized water until the conductivity and solution pH of the supernatant remained constant. The suspension was dried at 80 °C, the white powder (Zn–Al–OH binary hydroxide) as the absorbent precursor was obtained. The absorbent precursor was finally calcinated at 300 °C for 4 h, and the Zn–Al–O binary metal oxide was obtained.

2.3. Adsorbent characterization

A crystal phase analysis of the Zn–Al–O binary metal oxide was performed using an X-ray diffraction (XRD) diffractometer (D/max-TTR III, Rigaku, Japan) with copper Kα. The specific surface area, pore volume, and pore size distribution of the Zn–Al–O binary metal oxide were measured on an Automated Surface Area and Pore Size Analyzer (QuadraSorb SI, Quantachrome, USA) by nitrogen adsorption–desorption. The functional groups of the Zn–Al–O binary metal oxide were determined by Fourier transform infrared (FT-IR) spectra (Spectrum GX, PerkinElmer, USA) using a transmission model with the KBr pellet method. The zeta potentials of the Zn–Al–O binary metal oxide were determined by a Zetasizer (Zetasizer Nano, Malvern, UK). The composition of the Zn–Al–O, i.e., Zn and Al, was determined by inductively coupled plasma mass spectrometry (ICP-MS, Agilent 7500, USA) after acid digestion pretreatment.

2.4. Experimental procedure

The adsorption isotherm and predominant factor investigations were carried out with batch experiments. Each batch experiment was performed in a 500 mL glass vessel, with 100 mL of benzotriazole solution at different initial concentrations being used. The solution pH was adjusted with 0.1 mol L^{-1} H_2SO_4 or NaOH solution. The adsorption of benzotriazole on the Zn–Al–O binary metal oxide reached equilibrium within 30 min based on the adsorption kinetics results. Therefore, after the addition of the Zn–Al–O binary metal oxide, the suspension was mixed with a magnetic stirrer for 30 min. Samples were collected at predetermined time intervals and immediately filtered using 0.45 μm cellulose acetate membranes to separate the adsorbent from the supernatant. The residual benzotriazole concentrations were immediately analyzed.

A blank benzotriazole adsorption experiment without adsorbent was carried out to evaluate experimental uncertainties. The results showed that the loss of benzotriazole without adsorbent was less than 3%. To check reproducibility, all the adsorption experiments were carried out in duplicate. The relative deviations were less than 5%.

2.5. Analysis

Benzotriazole was analyzed by high performance liquid chromatography (HPLC, Agilent 1200, USA) with UV detection at 254 nm. The separation was performed with an Eclipse XDB-C_{18} column (150 mm × 4.6 mm, 5 μm, Agilent) using an isocratic elution of 50% water and 50% methanol at a flow rate of 1.0 mL min^{-1}. The detection limit of benzotriazole was approximately 80 ng L^{-1} and the relative standard deviation was approximately 1.78%.

3. Results and discussion

3.1. Adsorbent characteristics

Comparing the XRD patterns of the absorbent precursor and Zn–Al–O binary metal oxide (Fig. 1), it is confirmed that the adsorbent phase changed significantly after calcination at 300 °C. The Zn–Al–O binary metal oxide was not in a simple composite form of ZnO and Al_2O_3, but in a form of a ZnO solid solution into which Al was inserted. The Zn–Al–O binary metal oxide is a hexagonal system, and has a single phase with relatively narrow width diffraction peaks, indicating an excellent crystalloid. The average crystal sizes of the absorbent precursor and the Zn–Al–O binary metal oxide were estimated using Scherer's formula, and were 20.2 nm and 17.9 nm, respectively.

The surface area and porosity of the absorbent precursor and the Zn–Al–O binary metal oxide were determined using nitrogen adsorption–desorption isotherms (Fig. 2). The results showed that after calcination at 300 °C, both the surface area and pore volume of the Zn–Al–O binary metal oxide increased substantially, which could provide more active sites for pollutant adsorption. The isotherm of N_2 absorbed on the Zn–Al–O binary metal oxide was a typical IV-like adsorption isotherm with a hysteretic loop in the

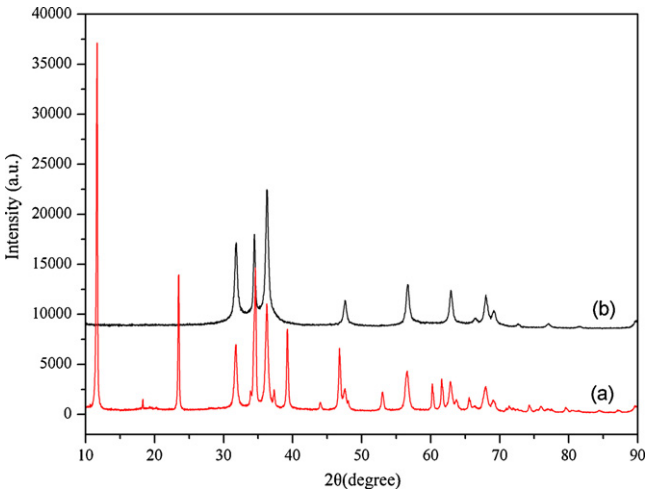

Fig. 1. XRD patterns of the absorbent precursor (a) and the Zn–Al–O binary metal oxide (b).

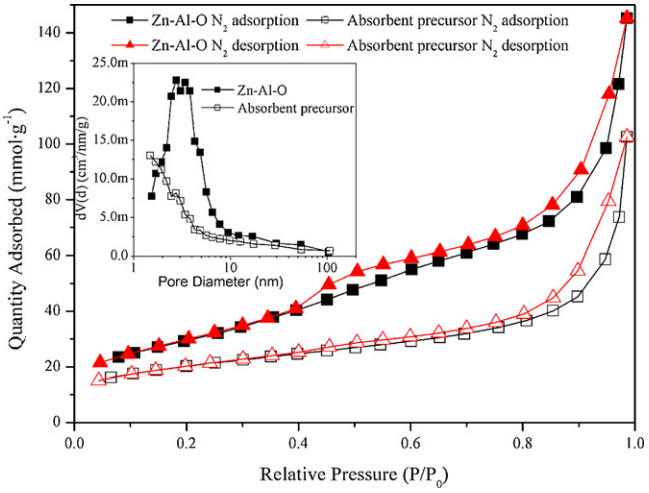

Fig. 2. N_2 adsorption–desorption isotherms and BJH pore size distribution curve of the absorbent precursor and Zn–Al–O binary metal oxide.

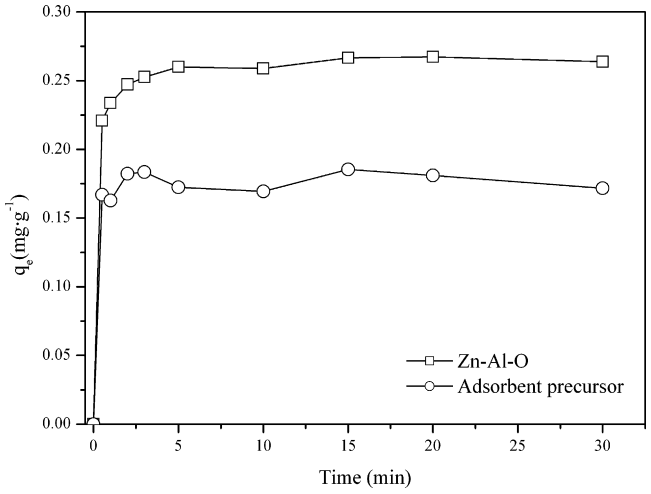

Fig. 4. Adsorptive capacity of benzotriazole by the absorbent precursor and Zn–Al–O binary metal oxide. Reaction conditions: pH = 6.0 ± 0.1, $T = 25 \pm 1\,^{\circ}C$, $[BTri]_0 = 5\ \mu mol\ L^{-1}$, and [adsorbent] = 5 g L^{-1}.

Table 1
BET results of Zn–Al–O binary metal oxide and its precursor.

	A_{BET} [a] ($m^2\ g^{-1}$)	V_{tal} [b] ($mL\ g^{-1}$)	D_{avg} [c] (nm)
Zn–Al–O	108	0.225	8.33
Adsorbent precursor	69.5	0.159	9.13

[a] The surface area of metal oxide calculate by BET model.
[b] The total pore volume of the metal oxide.
[c] The average diameter of the pore of the metal oxide.

range of 0.4–1.0 P/P_0, indicating the presence of mesoporous materials. The pore size distribution (Fig. 2) was determined using the Barrett–Joyner–Halenda (BJH) method from the desorption branch of the isotherm. The BET surface area, total pore volume and average pore diameter of both the absorbent precursor and Zn–Al–O binary metal oxide are shown in Table 1.

The FT-IR results of the absorbent precursor and the Zn–Al–O binary metal oxide are shown in Fig. 3. For the Zn–Al–O binary metal oxide, the adsorption bands at 3458 cm^{-1} and 1630 cm^{-1} corresponded to –OH stretching and bending vibrations, which were attributed to the adsorption of water molecules in the air and the existence of surface hydroxyl groups. The absorption peaks at 790 cm^{-1} and 431 cm^{-1} originated from Al–O and Zn–O vibrations, respectively [22,23]. Based on the changes in the –OH stretching and bending vibrations between the precursor and the binary metal oxide, it is suggested that calcination resulted in decreases of the surface hydroxyl group density on the metal oxide surface. As shown in Fig. 3, the peaks associated with Al–O and Zn–O vibrations were unclear and the relative peak intensity was weaker after calcination. These results confirmed that the Zn–Al–O binary metal oxide was not in a simple ZnO and Al_2O_3 composite form, but in a ZnO solid solution form.

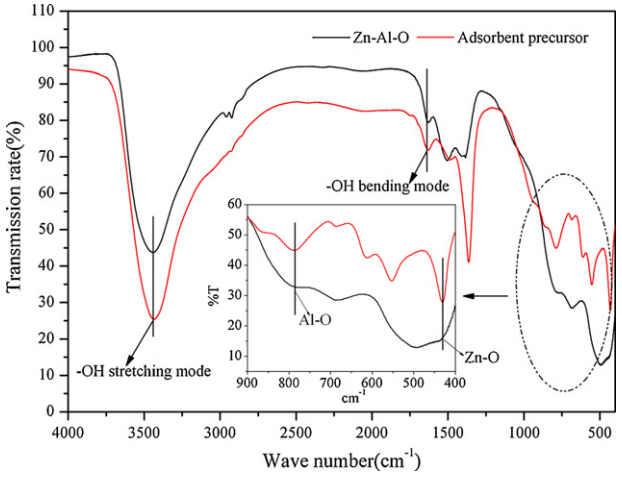

Fig. 3. FT-IR characterization of the absorbent precursor and Zn–Al–O binary metal oxide.

Based on the ICP-MS analysis results, the percentage composition of the Zn–Al–O was determined. Zn accounted for approximately 40.85% of the Zn–Al–O binary metal oxide, while Al accounted for approximately 11.14% of the total mass. Thus, the empirical formula for the composition of the Zn–Al–O could be expressed as $Zn_{1.53}AlO_{7.27}$.

3.2. Adsorption efficiency of benzotriazole

Efficiencies of benzotriazole adsorption onto Zn–Al–O binary metal oxide and the absorbent precursor are shown in Fig. 4. The Zn–Al–O binary metal oxide exhibited a fast adsorption rate and a good adsorption capacity for benzotriazole. The benzotriazole concentration decreased after the first contact with the adsorbent, and decreased to 12.6% in the first 5 min. The amount of adsorbed benzotriazole increased steeply from 0 to 0.26 mg g^{-1} during the same period. After 5 min, the removal efficiency remained constant. The overall removal efficiency and adsorption amount achieved were 88.7% and 0.264 mg g^{-1}, respectively.

The absorbent precursor also exhibited a rapid initial adsorption, but the benzotriazole removal efficiency and adsorption amount were only 57.7% and 0.172 mg g^{-1}, respectively, which were much lower than that of the Zn–Al–O binary metal oxide. This may be related to the different physical and chemical properties of the absorbent precursor and Zn–Al–O binary metal oxide. The smaller surface area and lower pore volume of the absorbent precursor probably led to the decrease in adsorption sites and adsorption amounts.

3.3. Effect of adsorbent dosage on benzotriazole adsorption

Different masses of the Zn–Al–O binary metal oxide were chosen to study the effect of adsorbent dosage on benzotriazole adsorption. Results are shown in Fig. 5. The amount of benzotriazole adsorbed increased with increasing adsorbent dosage. The adsorbed amounts were 0.162 mg g^{-1}, 0.221 mg g^{-1}, 0.264 mg g^{-1}

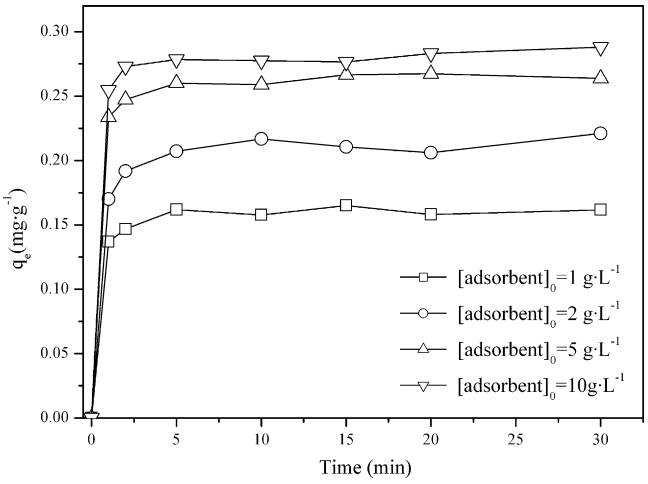

Fig. 5. Effect of adsorbent dosage on benzotriazole adsorption. Reaction conditions: pH = 6.0 ± 0.1, T = 25 ± 1 °C, and [BTri]$_0$ = 5 μmol L^{-1}.

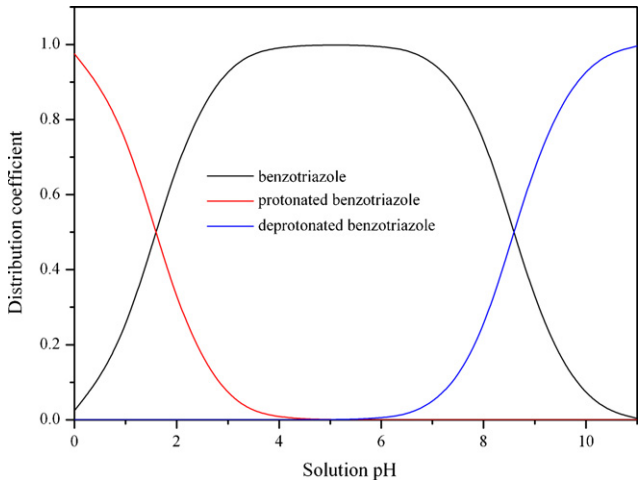

Fig. 7. Distribution of different benzotriazole species in water as a function of pH.

and 0.288 mg g^{-1} when the adsorbent was 1 g L^{-1}, 2 g L^{-1}, 5 g L^{-1}, and 10 g L^{-1}, respectively. The removal efficiency changed from 54.3%, 74.3%, and 88.7% to 96.8% at the corresponding reaction conditions. A larger amount of adsorbent would provide more adsorption sites, resulting in high levels of adsorbed benzotriazole and good removal efficiency.

3.4. Effect of solution pH on benzotriazole adsorption

The removal of benzotriazole as a function of solution pH is presented in Fig. 6. It is clear that little benzotriazole was adsorbed onto glass vessels surfaces at pH ranges from 3 to 11. The loss of benzotriazole through adsorption to glass vessels was less than 3% at any pH conditions, indicating that the adsorption by glass vessels could be ignored. Therefore, the benzotriazole adsorption was only caused by the Zn–Al–O binary metal oxide. The results also showed benzotriazole adsorption by the binary metal oxide was almost independent of pH. The adsorption amounts were at high levels for all pH values in the range of 4.0–11.0. The change in adsorption amount was less than 10% throughout the pH range. However, the adsorbed amount appeared to decrease slightly under strongly acidic condition (pH = 2.8), which was probably due to a reaction between the Zn–Al–O binary metal oxide and acid.

Benzotriazole is weak basic [7,24]. The pK_a values of its neutral and protonated species are 8.6 and 1.6, respectively [25]. Therefore,

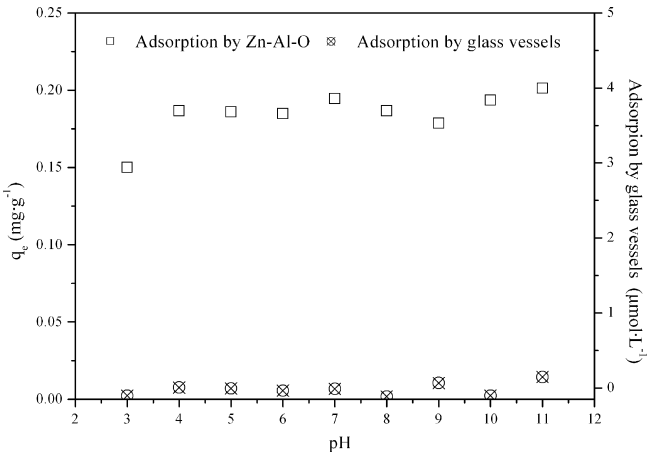

Fig. 6. Effect of solution pH on benzotriazole adsorption. Reaction conditions: T = 25 ± 1 °C, [BTri]$_0$ = 5 μmol L^{-1}, and [adsorbent] = 2 g L^{-1}.

it becomes positively or negatively charged due to protonation or deprotonation under different pH values (Eq. (1)) [26,27]:

$$BTAH_2^+ \overset{acid}{\longleftarrow} HBTA \overset{basic}{\longrightarrow} BTA^- \quad (1)$$

where HBTA indicates benzotriazole. Fig. 7 shows the predominant species of benzotriazole under different pH conditions. It is clear that the protonated benzotriazole, benzotriazole molecule and deprotonated benzotriazole were the predominant species when the solution pH was lower than 1.6, between 1.6 and 8.6, and greater than 8.6, respectively.

The surface of metal oxides can also become positively or negatively charged at different pH conditions. The surface charges are generated from the adsorption of H^+ and OH^- on the surface ionized group [28]. Eqs. (2) and (3) show the proton balance equations for metal oxides:

$$M\text{–}OH + H_3O^+ \overset{pH<pH_{IEP}}{\rightleftharpoons} M\text{–}OH_2^+ + H_2O \quad (2)$$

$$M\text{–}OH + H_2O \overset{pH>pH_{IEP}}{\rightleftharpoons} M\text{–}O^- + H_3O^+ \quad (3)$$

The pH at which the zeta potential equals zero is called isoelectric point (IEP). It can be used to qualitatively assess the surface charge on the adsorbent and characterize the protonation and deprotonation of the amphoteric surface functional groups [14,29]. The IEP of the Zn–Al–O binary metal oxide was determined to be 9.69 in this study (Fig. 8). Thus, when the pH was lower than 9.69, the Zn–Al–O binary metal oxide was protonated making it electropositive. When pH was greater than 9.69, the deprotonation occurred, resulting in an electronegative surface.

The surface charge properties of the adsorbate and adsorbent at different pH values resulted in multiple interactions occurring. Hydrogen-bond interactions occurred between the neutral forms of benzotriazole and the Zn–Al–O binary metal oxide, because they could act as hydrogen-bond donors or acceptors. Electrostatic interactions commonly occurred between the charged surface of the adsorbate and adsorbent. Additionally, ion exchange would also play a role in benzotriazole adsorption when only benzotriazole had surface charges. Thus, the minor changes in the benzotriazole adsorption capacity at the solution pH ranges from 4 to 11 probably indicates that the adsorption was due to the combination of multiple interactions based on the surface charge properties of the adsorbate and adsorbent.

3.5. Effect of ionic strength on benzotriazole adsorption

The effect of ionic strength on benzotriazole adsorption is shown in Fig. 9. Sodium nitrate ($NaNO_3$) was chosen as the electrolyte in

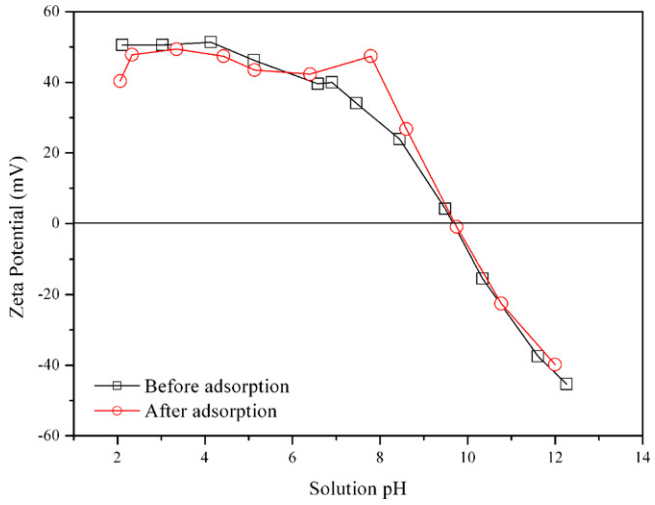

Fig. 8. Zeta potential of Zn–Al–O binary oxide before and after reaction with benzotriazole. Reaction conditions: $T = 25 \pm 1\,^{\circ}C$, $[BTri]_0 = 5\,\mu mol\,L^{-1}$, and [adsorbent] = $2\,g\,L^{-1}$.

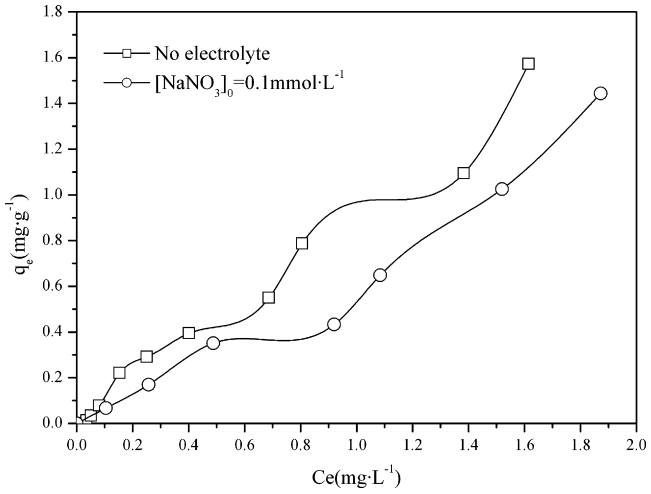

Fig. 10. Adsorption isotherms of benzotriazole on Zn–Al–O binary metal oxide with and without electrolyte. Reaction conditions: pH = 6.0 ± 0.1, $T = 25 \pm 1\,^{\circ}C$, and [adsorbent] = $2\,g\,L^{-1}$.

this study. The amount of adsorbed benzotriazole decreased with increasing $NaNO_3$ concentrations. The adsorbed amount decreased from 0.221 mg g^{-1} to 0.135 mg g^{-1} when the $NaNO_3$ concentration was increased from 0 mmol L^{-1} to 10 mmol L^{-1}. This indicates that the electrolyte competed with benzotriazole for adsorption sites and inhibited the benzotriazole adsorption.

There are two probable reasons for this competition. Under the reaction condition (pH = 6.0), the surface of the Zn–Al–O binary metal oxide may be positively charged or may still be neutral. Benzotriazole was probably in its neutral and protonated forms at the same solution pH. The surface charge properties of the adsorbent and adsorbate resulted in multiple interactions. When electrolytes were present, Na^+ and NO_3^- would compete with the neutral or protonated benzotriazole for adsorption sites and inhibit benzotriazole adsorption. On one hand, it was good for NO_3^- to be adsorbed onto the positively charged adsorbent by electrostatic interactions [30]. On the other hand, the hydrogen ion of the hydroxyl group on the Zn–Al–O binary metal oxide surface would exchange with Na^+ in solution due to ion exchange. Thus, the electrolyte preferred to occupy portion of the adsorption sites on the surface of the Zn–Al–O binary metal oxide, resulting in poor adsorption of benzotriazole.

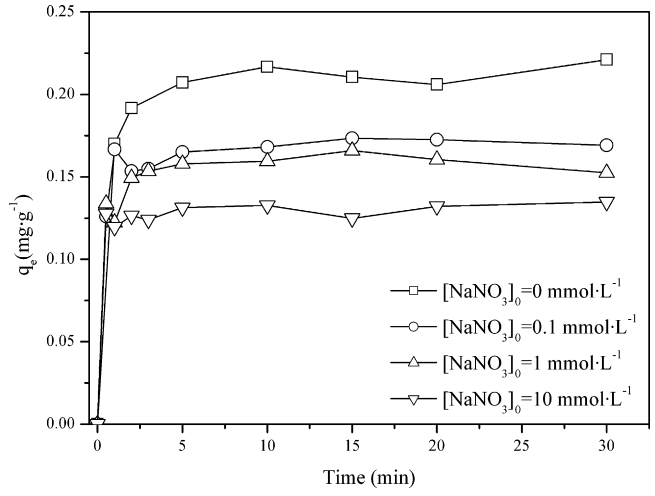

Fig. 9. Effect of ionic strength on benzotriazole adsorption. Reaction conditions: pH = 6.0 ± 0.1, $T = 25 \pm 1\,^{\circ}C$, $[BTri]_0 = 5\,\mu mol\,L^{-1}$, and [adsorbent] = $2\,g\,L^{-1}$.

3.6. Adsorption isotherm

The adsorption isotherms of benzotriazole onto the Zn–Al–O binary metal oxide with and without electrolytes at 25 °C are presented in Fig. 10. Based on the liquid-phase adsorption isotherm classification by Giles et al. [31], the adsorption isotherm of benzotriazole onto Zn–Al–O binary metal oxide without electrolytes was consistent with an S-type adsorption isotherm. When the $NaNO_3$ concentration was 0.1 mmol L^{-1}, the adsorption isotherm was still an S-type isotherm, but shifted to the right side due to the partial occupation of adsorption sites by the electrolyte.

Four adsorption isotherm models, i.e. the Langmuir [32], Freundlich [33], Dubinin–Radushkevich [34], and Temkin [35] models, were used to fit the equilibrium adsorption data. The linear forms of the four models are as follows:

$$\text{Langmuir isotherm}: \quad \frac{1}{q_e} = \frac{1}{q_m K_L C_e} + \frac{1}{q_m} \tag{4}$$

$$\text{Freundlich isotherm}: \quad \log_{10} q_e = \frac{1}{n} \log_{10} C_e + \log_{10} K_F \tag{5}$$

$$\text{Dubinin–Radushkevich isotherm}: \quad \ln(q_e) = \ln(q_m) - K_{DR}\varepsilon^2 \tag{6}$$

$$\varepsilon = RT \ln\left(1 + \frac{1}{C_e}\right) \tag{7}$$

$$\text{Temkin isotherm}: \quad q_e = \frac{RT}{b_T} \ln K_T C_e \tag{8}$$

where q_e is the amount of benzotriazole adsorbed onto the Zn–Al–O binary metal oxide per gram at equilibrium (mg g^{-1}); C_e is the residual concentration of benzotriazole in solution at equilibrium (mg L^{-1}); q_m is the maximum monolayer adsorption capacity (mg g^{-1}); K_L is the Langmuir isotherm constant related to the affinity between the adsorbent and the adsorbate (L g^{-1}); K_F is the Freundlich coefficient showing the adsorption capacity [(mg g^{-1})(L $mg^{-1})^{1/n}$]; n is the heterogeneity factor; K_{DR} is the porosity factor (mol^2 J^{-2}); ε is the Polanyi potential; R is the universal gas constant with a value of 8.314 J mol^{-1} K^{-1}; T is the absolute temperature (K); b_T is the adsorption potential of the Zn–Al–O binary metal oxide (kJ mol^{-1}); and K_T is the equilibrium constant corresponding to maximum binding energy (L g^{-1}).

The parameters of the four isotherms are summarized in Table 2. It shows that the isotherm data were best fitted Langmuir isotherm when compared to other three isotherms based on the high coefficient of determination ($r^2 = 0.992$). The maximum

Table 2
Isotherm model parameters for benzotriazole adsorption on Zn–Al–O[a].

Isotherm model	Isotherm equation	Model constants	No electrolyte	Electrolyte[b]
Langmuir	$\frac{1}{q_e} = \frac{1}{q_m K_L C_e} + \frac{1}{q_m}$	q_m (mg g^{-1})	9.51	7.30
		K_L (L g^{-1})	0.103	0.932
		r^2	0.992	0.973
Freundlich	$\log_{10} q_e = \frac{1}{n}\log_{10} C_e + \log_{10} K_F$	K_F [(mg g^{-1})(L mg^{-1})$^{1/n}$]	0.907	0.643
		n	1.11	1.00
		r^2	0.974	0.978
Dubinin–Radushkevich	$\ln(q_e) = \ln(q_m) - K_{DR}\varepsilon^2$	q_m (mg g^{-1})	1.07	0.867
		K_{DR} (mol^2 kJ^{-2})	0.065	0.819
	$\varepsilon = RT \ln\left(1 + \frac{1}{C_e}\right)$	E (kJ mol^{-1})	−2.77	−2.47
		r^2	0.918	0.866
Temkin	$q_e = \left(\frac{RT}{b_T}\right)\ln(K_T) + \left(\frac{RT}{b_T}\right)\ln(C_e)$	K_T (mol g^{-1})	9.63	6.79
		b_T (kJ mol^{-1})	5.73	6.05
		r^2	0.816	0.751

[a] Reaction conditions: pH = 6.0 ± 0.1, T = 25 ± 1 °C, and [adsorbent] = 2 g L^{-1}.
[b] Electrolyte: $[NaNO_3]_0$ = 0.1 mmol L^{-1}.

monolayer adsorption capacity of benzotriazole was 9.51 mg g^{-1} with no electrolytes, and decreased to 7.30 mg g^{-1} in the presence of 0.1 mmol L^{-1} $NaNO_3$. Freundlich coefficients without and with electrolytes were 0.907 and 0.643 (mg g^{-1})(L mg^{-1})$^{1/n}$, respectively. Heterogeneity factors without and with electrolytes were 1.11 and 1.00, respectively.

Based on the isotherm data, it suggests that the Zn–Al–O binary metal oxide has great potential for the application in removal of trace amounts of benzotriazole from water. The adsorbent dosage should be increased when applied to compensate for the effects of electrolytes in water and meet the treatment needs. Dubinin–Radushkevich isotherm model was used to determine the characteristic porosity and the apparent free energy of adsorption, while Temkin isotherm model was used to determine the adsorption potentials of the adsorbent for adsorbates. Both of these models had less precise coefficients than those obtained from Langmuir and Freundlich isotherms (Table 2). The results also indicate that the presence of electrolytes would inhibit benzotriazole adsorption onto the Zn–Al–O binary metal oxide.

3.7. Adsorption kinetics

The kinetics of benzotriazole adsorption onto the Zn–Al–O binary metal oxide is shown in Fig. 11. The adsorption process can be divided into a rapid step and a slow one. Instantaneous adsorption occurred in all cases, indicating that the initial adsorption of benzotriazole by the Zn–Al–O binary metal oxide probably took place via external surface adsorption [36,37]. The slow adsorption step represented a gradual uptake of benzotriazole at the inner surface [20,38]. However, the slow step was insignificant for lower initial concentrations of benzotriazole.

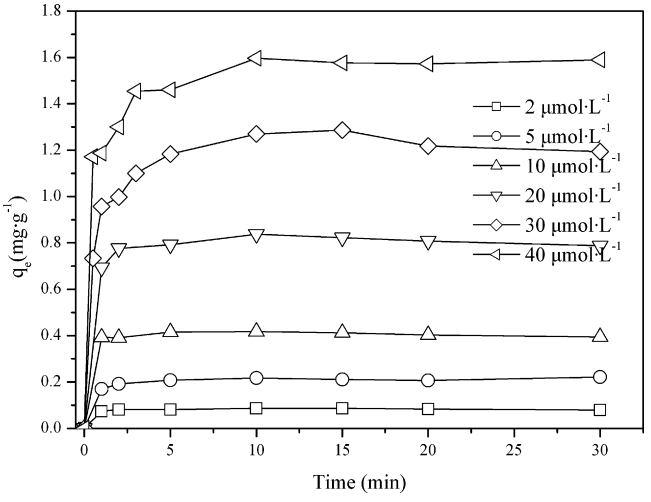

Fig. 11. Effect of contact time on benzotriazole adsorption under different initial concentrations. Reaction conditions: pH = 6.0 ± 0.1, T = 25 ± 1 °C, and [adsorbent] = 2 g L^{-1}.

Four kinetics models, including pseudo-first-order model [39], pseudo-second-order model [40,41], Elovich equation [42] and intraparticle diffusion model [43] were used to describe the adsorption process, of which the linear forms are as follows:

$$\text{Pseudo-first order equation}: \quad \ln(q_e - q_t) = \ln(q_e) - k_1(t) \tag{9}$$

$$\text{Pseudo-second order equation}: \quad \frac{t}{q_t} = \frac{1}{h} + \frac{1}{q_e}t \tag{10}$$

$$h = k_2 q_e^2 \tag{11}$$

$$\text{Elovich model}: \quad q_t = \frac{1}{\beta}\ln(\alpha\beta) + \frac{1}{\beta}\ln(t) \tag{12}$$

$$\text{Intraparticle diffusion model}: \quad q_t = k_p t^{1/2} + C \tag{13}$$

$$\ln\left[1 - \left(\frac{q_t}{q_e}\right)^2\right] = -\frac{\pi^2 D}{r^2}t \tag{14}$$

where q_t is the amount of benzotriazole adsorbed onto the Zn–Al–O binary metal oxide per gram at any time t (mg g^{-1}); q_e is the amount of benzotriazole adsorbed at equilibrium (mg g^{-1}); k_1 is the rate constant of the pseudo-first order model (min^{-1}); k_2 is the rate constant of the pseudo-second order model (g mg^{-1} min^{-1}); h is the initial adsorption rate of the pseudo-second order model (mg g^{-1} min^{-1}); α is the adsorption velocity constant for benzotriazole (mg g^{-1} min^{-1}); β is the desorption constant (g mg^{-1}); k_p is the intraparticle diffusion constant (mg g^{-1} min$^{-1/2}$); and C is the intercept of the line which is proportional to the boundary layer thickness.

The kinetic parameters depend on different initial concentrations of benzotriazole, and are summarized in Table 3. The data obtained from the pseudo-first-order model was not applicable for describing benzotriazole adsorption onto the Zn–Al–O binary metal oxide. The calculated adsorption amount obtained from pseudo-first-order kinetic model did not give acceptable values. The high coefficient of determination ($r^2 > 0.95$) confirmed that benzotriazole adsorption onto the Zn–Al–O binary metal oxide was well represented by the pseudo-second-order kinetics model. The calculated amount of benzotriazole adsorbed at equilibrium agreed with the experimental data. The rate constant of pseudo-second order

Table 3
Kinetic parameters of benzotriazole adsorption by Zn–Al–O binary metal oxide[a].

Concentrations ($mg\,L^{-1}$)	Pseudo-first order				Pseudo-second order				Elovich equation			Intraparticle diffusion		
	$q_{e,exp}$ ($mg\,g^{-1}$)	$q_{e,cal}$ ($mg\,g^{-1}$)	k_1 (min^{-1})	r^2	$q_{e,cal}$ ($mg\,g^{-1}$)	k_2 ($g\,mg^{-1}\,min^{-1}$)	$h = k_2 q_e^2$ ($mg\,g^{-1}\,min^{-1}$)	r^2	α ($mg\,g^{-1}\,min^{-1}$)	β ($g\,mg^{-1}$)	r^2	k_p ($mg\,g^{-1}\,min^{-1/2}$)	C	r^2
0.238	0.073	0.038	0.541	0.812	0.069	49.6	0.236	0.965	2.75	18.4	0.995	0.0232	0.0272	0.906
0.595	0.221	0.082	0.279	0.786	0.163	27.0	0.717	0.995	2.73	5.86	0.996	0.0261	0.134	0.927
1.19	0.354	0.149	0.394	0.745	0.277	13.7	1.05	0.978	2.77	3.61	0.994	0.0786	0.173	0.812
2.38	0.794	0.399	0.730	0.789	0.863	1.89	1.41	0.955	2.83	1.71	0.997	0.234	0.271	0.690
3.57	1.29	0.474	0.329	0.931	1.316	1.67	2.89	0.998	2.77	1.04	0.993	0.173	0.767	0.692
4.76	1.59	0.460	0.232	0.940	1.622	1.46	3.84	0.998	2.74	0.728	0.998	0.169	1.04	0.960
5.95	2.20	0.700	0.177	0.842	2.10	0.920	4.06	0.999	2.76	0.624	0.993	0.187	1.38	0.938

[a] Reaction conditions: pH = 6.0 ± 0.1, T = 25 ± 1 °C, [adsorbent] = 2 g L^{-1}.

model decreased with increasing initial concentrations of benzotriazole. The adsorption amount increased from 0.069 mg g^{-1} to 2.10 mg g^{-1} as the initial concentrations of benzotriazole increased from 0.238 mg L^{-1} to 5.95 mg L^{-1}, indicating that the Zn–Al–O binary metal oxide was good for removing the polar contaminant benzotriazole from water. It was noted that the initial adsorption rate increased from 0.236 mg g^{-1} min^{-1} to 4.06 mg g^{-1} min^{-1} as the initial concentrations of benzotriazole increased from 0.238 mg L^{-1} to 5.95 mg L^{-1}, suggesting that high initial concentrations would enhance the adsorption process.

Elovich equation was the most applicable for describing benzotriazole adsorption onto the Zn–Al–O binary metal oxide as the coefficient of determination was greater than 0.99. The adsorption velocity constant (α) was quite similar under different initial concentrations, but the desorption constant (β) decreased from 18.4 g mg^{-1} to 0.624 g mg^{-1} as the initial concentrations of benzotriazole increased from 0.238 mg L^{-1} to 5.95 mg L^{-1}. This result suggests that adsorbate molecules that had adsorbed onto the adsorbent surface could inhibit desorption and promote adsorption.

Due to the porosity of the Zn–Al–O binary metal oxide, the intraparticle diffusion kinetic model was expected to have a role in the adsorption process. Boundary layer diffusion and intraparticle diffusion effects would occur during the adsorption process based on relationships between the adsorption capacity and the square root of the contact time (data not shown here) [20,38]. The diffusion driving force increased with increasing initial benzotriazole concentrations, which resulted in the intraparticle diffusion constant increasing except for the initial concentration of benzotriazole being 2.38 mg L^{-1}.

3.8. Adsorption mechanism

For adsorption onto a solid surface, the adsorption mechanisms may include electrostatic interactions, ion exchange, hydrogen bonding, hydrophobic interactions or other else [44]. Based on the characteristics of the adsorbate and adsorbent, the mechanism of benzotriazole adsorption by the Zn–Al–O binary metal oxide was very complex. Benzotriazole adsorption was thought to mainly take place via surface adsorption. After adsorption sites were occupied, benzotriazole molecules would diffuse into the pores of the Zn–Al–O binary metal oxide for further adsorption. The surface adsorption mechanisms can be explained by electrostatic interactions, ion exchange and hydrogen-bond interactions at different pH values.

Benzotriazole is an ionized organic pollutant, while the Zn–Al–O binary metal oxide has an amphoteric surface. Thus, both the adsorbate and adsorbent may have multiple species in the solution due to their surface charge properties at different pH values. As seen in Table 4, electrostatic interactions that commonly occurred between the different charged surfaces of the adsorbate and adsorbent probably occurred at pH values ≤ 8.6 (Eq. (15)) and pH < 9.69 (Eq. (16)):

$$M\text{–}O^- + BTAH_2^+ \rightarrow M\text{–}O^- \cdots BTAH_2^+ \quad (15)$$

$$M\text{–}OH_2^+ + BTA^- \rightarrow M\text{–}OH_2^+ \cdots BTA^- \quad (16)$$

However, the IEP showed almost no decrease before and after the adsorption reaction (shifting from 9.69 to 9.66), suggesting that the presence of benzotriazole did not make the adsorbent surface more positively or negatively charged in this study. The very minor change in the IEP may indicate that electrostatic interactions were not the main mechanism of benzotriazole adsorption onto the adsorbent.

Ion exchange would have a role in benzotriazole adsorption when only the benzotriazole was surface charged. The Zn–Al–O binary metal oxide had surface hydroxyl groups that could be con-

Table 4
Probable species forms and presumed interactions under different solution pH values.

pH condition	Probable species of adsorbent	Probable species of adsorbate	Presumed interactions
$pH \geq 9.69$	$M–O^-$ M–OH	BTA^- HBTA	$M–OH + HBTA \rightarrow M–OH \cdots BTA$ $M–OH + BTA^- \rightarrow M–BTA + OH^-$
$8.6 < pH < 9.69$	$M–O^-$ M–OH $M–OH_2^+$	BTA^- HBTA	$M–OH + HBTA \rightarrow M–OH \cdots HBTA$ $M–OH + BTA^- \rightarrow M–BTA + OH^-$ $M–OH_2^+ + BTA^- \rightarrow M-OH_2^+ \cdots BTA^-$ $M–OH + HBTA \rightarrow M–OH \cdots HBTA$
$pH \leq 8.6$	$M–O^-$ M–OH $M–OH_2^+$	BTA^- HBTA $BTAH_2^+$	$M–OH + BTAH_2^+ \rightarrow M–OBTAH_2 + H^+$ $M–OH + BTA^- \rightarrow M–BTA + OH^-$ $M–OH_2^+ + BTA^- \rightarrow M–OH_2^+ \cdots BTA^-$ $M–O^- + BTAH_2^+ \rightarrow M–O^- \cdots BTAH_2^+$

verted into ion exchangers in solution. Thus, the hydrogen ion of the surface hydroxyl groups would exchange with protonated benzotriazole at $pH \leq 8.6$ (Eq. (17)). In addition, the neutral surface hydroxyl groups may also exchange with deprotonated benzotriazole (Eq. (18)):

$$M–OH + BTAH_2^+ \rightarrow M–OBTAH_2 + H^+ \quad (17)$$

$$M–OH + BTA^- \rightarrow M–BTA + OH^- \quad (18)$$

$$M–OH + HBTA \rightarrow M–OH \cdots HBTA \quad (19)$$

Finally, hydrogen-bond interactions were considered to be the main adsorption mechanism (Eq. (19)). Both benzotriazole and the Zn–Al–O binary metal oxide could act as hydrogen-bond donors or acceptors due to the imido group of the benzotriazole and hydroxyl groups on the Zn–Al–O binary metal oxide surface (Fig. 12). Hydrogen atoms of the surface hydroxyl groups could interact with the nitrogen atoms of the imido groups of benzotriazole to form hydrogen bonds. Because there is a lone pair of electrons on a oxygen atom of the water molecule, the surface hydroxyl groups on the adsorbent could also interact with that oxygen atoms to form hydrogen bonds. The electro-negativity of the oxygen atom is greater than that of the nitrogen atom, so it is much easier for the surface hydroxyl groups to form hydrogen bonds with water molecules. That is, water molecules competed for adsorption sites with benzotriazole during the adsorption process. The oxygen atoms of adsorbed water molecules would also interact with the nitrogen atoms of the imido groups to form hydrogen bonds, promoting benzotriazole adsorption. Moreover, the benzotriazole molecule could also form hydrogen bond with another benzotriazole molecule, leading to synergistic adsorption.

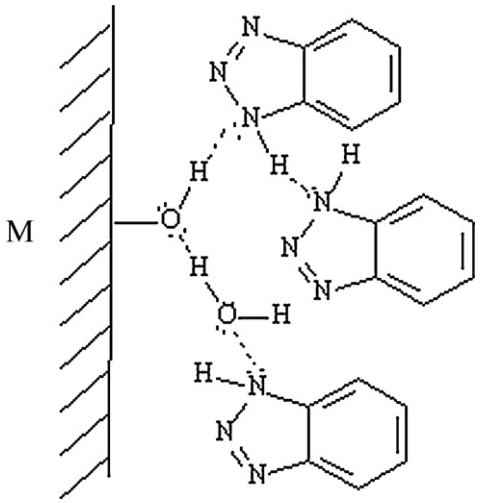

Fig. 12. Possible hydrogen-bond interaction of benzotriazole adsorption on Zn–Al–O binary oxide.

4. Conclusions

Based on above experimental results, the following conclusions can be drawn:

(1) The Zn–Al–O binary metal oxide has great potential for application in removal of trace amounts of polar benzotriazole from water. Benzotrizole adsorption was almost independent of pH. The adsorption amount increased with increasing adsorbent dosage and initial benzotriazole concentration, but decreased with increasing ionic strength in the water.
(2) Langmuir isotherm model provided the best fit for the adsorption behavior of benzotriazole onto Zn–Al–O binary metal oxide. Elovich equation and pseudo-second-order kinetic models were more applicable for describing the adsorption process.
(3) Benzotriazole adsorption was primarily via the surface adsorption. The surface adsorption mechanisms are likely to be a combination of electrostatic, ion exchange and hydrogen-bond interactions.

Acknowledgments

The research was supported by the Natural Science Foundation of China (40903038), the China's national basic research program (2008CB418200) and China Postdoctoral Science Foundation (20090450458).

The authors thank the anonymous reviewers for their helpful and constructive suggestions. And the authors also thank Dr. Yingchen Bai and Dr. Fei Qi for the discussion of the issues.

References

[1] M. la Farre, S. Perez, L. Kantiani, D. Barcelo, Fate and toxicity of emerging pollutants, their metabolites and transformation products in the aquatic environment, Trends Anal. Chem. 27 (2008) 991–1007.
[2] D.A. Pillard, J.S. Cornell, D. Dufresne, M.T. Hernandez, Toxicity of benzotriazole and benzotriazole derivatives to three aquatic species, Water Res. 35 (2001) 557–560.
[3] W. Giger, C. Schaffner, H.P.E. Kohler, Benzotriazole and tolytriazole as aquatic contaminants. 1. Input and occurrence in rivers and lakes, Environ. Sci. Technol. 40 (2006) 7186–7192.
[4] D.A. Cancilla, J. Martinez, G.C. Van Aggelen, Detection of aircraft deicing/antiicing fluid additives in a perched water monitoring well at an international airport, Environ. Sci. Technol. 32 (1998), 3838-3835.
[5] D.A. Cancilla, A. Holtkamp, L. Mattassa, X. Fang, Isolation and characterization of Microtox TM-active components from aircraft de-icing/anti-icing solutions, Environ. Toxicol. Chem. 16 (1997) 430–434.
[6] D.S. Hart, L.C. Davis, L.E. Erickson, T.M. Callender, Sorption and partitioning parameters of benzotriazole compounds, Microchem. J. 77 (2004) 9–17.
[7] S. Weiss, J. Jakobs, T. Reemtsma, Discharge of three benzotriazole corrosion inhibitors with municipal wastewater and improvements by membrane bioreactor treatment and ozonation, Environ. Sci. Technol. 40 (2006) 7193–7199.
[8] S. Weiss, T. Reemtsma, Determination of benzotriazole corrosion inhibitors from aqueous environmental samples by liquid chromatography–electrospray ionization–tandem mass spectrometry, Anal. Chem. 77 (2005) 7415–7420.
[9] T. Reemtsma, U. Miehe, U. Duennbier, M. Jekel, Polar pollutants in municipal wastewater and the water cycle: occurrence and removal of benzotriazoles, Water Res. 44 (2010) 596–604.

[10] S.D. Richardson, T.A. Ternes, Water analysis: emerging contaminants and current issues, Anal. Chem. 77 (2005) 3807–3838.
[11] H. Zeng, M. Arashiro, D.E. Giammar, Effects of water chemistry and flow rate on arsenate removal by adsorption to an iron oxide-based sorbent, Water Res. 42 (2008) 4629–4636.
[12] K. Banerjee, G.L. Amy, M. Prevost, S. Nour, M. Jekel, P.M. Gallagher, C.D. Blumenschein, Kinetic and thermodynamic aspects of adsorption of arsenic onto granular ferric hydroxide (GFH), Water Res. 42 (2008) 3371–3378.
[13] T. Tuutijärvi, J. Lu, M. Sillanpää, G. Chen, As(V) adsorption on maghemite nanoparticles, J. Hazard. Mater. 166 (2009) 1415–2142.
[14] Y. Li, B. Gao, T. Wu, D. Sun, X. Li, B. Wang, F. Lu, Hexavalent chromium removal from aqueous solution by adsorption on aluminum magnesium mixed hydroxide, Water Res. 43 (2009) 3067–3075.
[15] D. Dong, L. Liu, X. Hua, Y. Lu, Comparison of lead, cadmium, copper and cobalt adsorption onto metal oxides and organic materials in natural surface coatings, Microchem. J. 85 (2007) 270–275.
[16] M. Streat, K. Hellgardt, N.L.R. Newton, Hydrous ferric oxide as an adsorbent in water treatment. Part 3: Batch and mini-column adsorption of arsenic, phosphorus, fluorine and cadmium ions, Process Safety Environ. Protect. 86 (2008) 21–30.
[17] K. Ada, A. Ergene, S. Tan, E. Yalçın, Adsorption of Remazol Brilliant Blue R using ZnO fine powder: equilibrium, kinetic and thermodynamic modeling studies, J. Hazard. Mater. 165 (2009) 637–644.
[18] S. Pirillo, M.L. Ferreira, E.H. Rueda, The effect of pH in the adsorption of alizarin and eriochrome blue black R onto iron oxides, J. Hazard. Mater. 168 (2009) 168–178.
[19] S.S. Tripathy, J. Bersillon, K. Gopal, Removal of fluoride from drinking water by adsorption onto alum-impregnated activated alumina, Sep. Purif. Technol. 50 (2006) 310–317.
[20] K. Biswas, S.K. Saha, U.C. Ghosh, Adsorption of fluoride from aqueous solution by a synthetic iron (III)–aluminum (III) mixed oxide, Ind. Eng. Chem. Res. 46 (2007) 5346–5356.
[21] K. Biswas, K. Gupta, U.C. Ghosh, Adsorption of fluoride by hydrous iron(III)–tin(IV) bimetal mixed oxide from the aqueous solutions, Chem. Eng. J. 149 (2009) 196–206.
[22] K.E. Lipinska-Kalita, Infrared spectroscopic investigation of structure and crystallization of aluminosilicate glasses, J. Non-Cryst. Solids 119 (1990) 310–317.
[23] T. Ishikawa, K. Matsumoto, K. Kandori, T. Nakayama, Synthesis of layered zinc hydroxide chlorides in the presence of Al (III), J. Solid State Chem. 179 (2006) 1110–1118.
[24] C.L. Gruden, S.M. Dow, M.T. Hernandez, Fate and toxicity of aircraft deicing fluid additives through anaerobic digestion, Water Environ. Res. 73 (2001) 72–79.
[25] H.E. Toma, R.C. Rocha, Linkage isomerization reactions, Croat. Chem. Acta 74 (2001) 499–528.
[26] D. Tromans, R.H. Sun, Anodic polarization behavior of copper in aqueous chloride benzotriazole solutions, J. Electrochem. Soc. 138 (1997) 3235–3244.
[27] Y. Jia, P. Aagaard, G.D. Breedveld, Sorption of triazoles to soil and iron minerals, Chemosphere 67 (2007) 250–258.
[28] W. Stumm, Chemistry of the Solid–Water Interface, Wiley & Sons Inc., New York, 1992.
[29] A. Olgun, N. Atar, Equilibrium and kinetic adsorption study of Basic Yellow 28 and Basic Red 46 by a boron industry waste, J. Hazard. Mater. 161 (2009) 148–156.
[30] K.F. Hayes, C. Papelis, J.O. Leckie, Modeling ionic strength effects on anion adsorption at hydrous oxide/solution interfaces, J. Colloid Interface Sci. 125 (1988) 717–726.
[31] C.H. Giles, D. Smith, A. Huitson, A general treatment and classification of the solute adsorption isotherm: I. Theoretical, J. Colloid Interface Sci. 47 (1974) 755–765.
[32] I. Langmuri, The adsorption gases on plane surfaces of glass, mica and platinum, J. Am. Chem. Soc. 40 (1918) 1361–1368.
[33] H.M.F. Freundlich, Over the adsorption in solution, J. Phys. Chem. 57 (1906) 385–470.
[34] M.M. Dubinin, L.V. Radushkevich, The equation of the characteristic curve of activated charcoal, Proc. Acad. Sci. USSR: Phys. Chem. Sect. 55 (1947) 331.
[35] M.I. Temkin, V. Pyzhev, Kinetics of ammonia synthesis on promoted iron catalyst, Acta Physiochim. URSS 12 (1940) 327–356.
[36] D. Mohan, V.K. Gupta, S.K. Srivastava, S. Chander, Kinetics of mercury adsorption from wastewater using activated carbon derived from fertilizer waste material, Colloids Surf. A 177 (2001) 169–181.
[37] D. Mohan, K.P. Singh, Single- and multi-component adsorption of cadmium and zinc using activated carbon derived from bagasse—an agricultural waste, Water Res. 36 (2002) 2304–2318.
[38] M.A. Al-Ghouti, M.A.M. Khraisheh, M.N.M. Ahmad, S. Allen, Adsorption behaviour of methylene blue onto Jordanian diatomite, J. Hazard. Mater. 165 (2009) 589–598.
[39] C. Lagergren, About the theory of so called adsorption of soluble substances, Kung, Sven. Hand. 24 (1898) 171–177.
[40] Y.S. Ho, G. McKay, Kinetic models for the sorption of dye from aqueous solution by wood, Process Safety Environ. Protect. 76 (1998) 183–191.
[41] Y.S. Ho, G. McKay, The kinetics of sorption of divalent metal ions onto sphagnum moss peat, Water Res. 34 (2000) 735–742.
[42] S.H. Chien, W.R. Clayton, Application of Elovich equation to the kinetics of phosphate release and sorption in soils, Soil Sci. Soc. Am. J. 44 (1980) 265–268.
[43] W.J. Weber Jr., J.C. Morriss, Kinetics of adsorption on carbon from solution, J. Sanit. Eng. Div. Am. Soc. Civil Eng. 89 (1963) 31–60.
[44] M. Lu, G. Roam, J. Chen, C. Huang, Adsorption characteristics of dichlorvos onto hydrous titanium dioside surface, Water Res. 30 (1996) 1670–1676.